Journal of Applied Electrochemistry (2006) 36:499–505
DOI 10.1007/s10800-005-9106-7

Formation of nanocrystalline Zinc on ITO and Silicon substrates by electrochemical deposition

BEATRIZ H. JUÁREZ[1] and CONCEPCIÓN ALONSO[2,*]
[1]*Instituto de Ciencia de Materiales de Madrid (CSIC), Cantoblanco, 28049 Madrid, Spain*
[2]*Alonso, Dpto. Química Física Aplicada, Universidad Autónoma de Madrid, Cantoblanco, 28049 Madrid, Spain*
*(*author for correspondence, fax: + 33-91-497-47-85, e-mail: Concepcion.Alonso@uam.es)*

Received 2 September 2005; accepted in revised form 24 November 2005

Key words: cyclic voltammetry, electrodeposition, nanocrystalline, pulsating overpotential, Zinc

Abstract

Zn was deposited by means of cyclic voltammetry (CV) and square wave pulsating overpotential (OP) methods on ITO (indium tin oxide) and n-doped silicon (n-Si) substrates from an acetate-based electrolyte at two different temperatures in the absence of additives. The surface morphology of the Zn deposits was studied by scanning electron microscopy (SEM). The preferred orientation and the average size of the Zn electrodeposited particles on n-Si substrates were obtained by X-ray diffraction and the microhardness of the deposits was measured by standard means. The results show that the grain size of the electrodeposits increases as the temperature rises, and on the other hand that the PO method yields smaller grains and higher hardness values compared with those obtained by CV, irrespective of the temperature. Furthermore, in PO conditions a preferential (101) orientation is obtained for the growth of the Zn electrodeposits, but for long deposition times the growth direction is that [100] corresponding to the basal plane (002).

1. Introduction

Research on Zn electrodeposition has been extensively reported in widely varying conditions using a range of electrodes, analysing the dependence of the morphology on bath conditions and electrodeposition parameters [1]. The aqueous electrolytes most frequently used are sulphate [2, 3], chloride [4] or acetate [5] based with different pH values and in the presence of trace metals [3]. The metallic substrates used as cathodes include aluminium [3], steel [4, 6–8], carbon [4], zinc [7, 9] and copper [4, 10], among others. The electrochemical methods applied to deposit Zn have been constant potential [4, 8], current density [3, 6, 9], pulsed current [11] and pulsed potential [5].

The addition of organic compounds to the electrolytic baths can modify deposit characteristics such as structure, morphology, porosity and grain size [12–14]. In fact, a reduction in the grain size implies an increase in the hardness of the deposit [6], and thus an improvement in its mechanical properties. However, the development of the texture and morphology of electrodeposited Zn and their variation with electrochemical parameters remains unclear. Yim et al. [15] observed a decreasing basal plane (200) with increasing current density in an acid bath. Saber et al. [6] obtained a transition in the preferential orientation of the deposits by increasing the current density from pyramidal to high angle (112) to pyramidal (101) passing through prismatic (110). Raeissi et al. [16] deduced that changes in electrodeposition parameters such as the temperature, pH and current density have an influence on the nucleation and growth mechanisms of the Zn deposits and thus on their texture.

In this work, Zn has been deposited by means of electrochemical methods on n-doped Si and ITO (indium tin oxide) substrates from an acetate-based electrolyte at two different temperatures in the absence of additives. Several differences have been observed between samples obtained by the linear cyclic voltammetry (CV) or square wave pulsating potential (PO) methods, leading to the production of metallic deposits with different morphology, texture, grain size and hardness on semiconductor substrates.

2. Experimental

2.1. *Substrates*

ITO coated glass ($R = 2\ \Omega\ cm^{-1}$) and n-Si (111) surfaces were used as conducting substrates. Si substrates were cleaved from highly doped n-wafers ($R < 20\ \Omega\ cm^{-1}$). The native oxide was removed with 1% vol. HF solution for 10 min and finally rinsed with double deionised water. ITO and SiO_2-free n-Si substrates were hydrophilised following a method previously

described [17]. The back side of the Si samples was isolated from the electrolyte by painting with an insulator paste. Zn electrodeposition has been previously carried out in porous matrices by means of CV and PO approaches [17].

2.2. *Deposition of metallic Zn*

A three-electrode set-up was used for Zn electrodeposition. A platinum plate served as the auxiliary electrode. All the potentials are quoted with respect to a Ag/AgCl reference electrode. The cell was properly de-aerated by 99.999% N_2 for 20 min before each experiment. The Zn solution (100 g l^{-1}) was prepared from Zinc acetate, $ZnAc_2$, (Aldrich 99.95%) and ultrapure water (Millipore 18.2 MΩ). The pH of the solution was 6.3. The experiments were performed in a solution thermostated at 25 °C and 30 ± 0.5 °C with the help of a thermostatic bath.

Two different methods were used to obtain metallic Zn: CV and PO. In the case of samples grown on n-Si by CV, the potential range was −1.05 and −1.35 V at a scan rate of 10 mV s^{-1}. In the case of ITO samples, Zn electrodeposition was carried out between −0.850 and −1.055 V, at a scan rate of 10 mV s^{-1}. The pulsed potential waveform applied for Zn deposition on n-Si substrates was $E_{deposition} = -1.8$ V for $t_d = 1$ ms and $E_{off} = -1.05$ V for 10 ms. The pause-to-pulse ratio was 10 and the frequency was 90.9 Hz. For samples on ITO substrates $E_{deposition} = -1.05$ V and $E_{off} = -0.85$ V.

Deposition was carried out with gentle stirring by bubbling nitrogen through the solution, to prevent oxygen diffusion during the long electrolysis times. The deposition times (t_D) varied between 2 and 100 h.

2.3. *Characterisation*

A Philips scanning electron microscope (model XL30) was used to characterise the surface morphology of the Zn electrodeposits. An energy-dispersive X-ray analyser (model DX4i) equipped on the SEM was used to determine the compositions. X-ray diffraction analysis was carried out by using a Siemens diffractometer (model D5000) working with Cu $K\alpha_1$ radiation ($\lambda = 1.54056$ Å) and Cu $K\alpha_2$ radiation ($\lambda = 1.54439$ Å). The X-ray scan rate was 0.02° s^{-1} and 2θ-diffraction patterns were recorded in the 30–100° range. To determine the grain size and the preferential orientation of the Zn electrodeposits, the spectra were collected with a grazing angle in order to eliminate the contribution of the substrates.

The microhardness of the Zn electrodeposits was measured using a FM microhardness tester with a pyramidal indenter. A load of 10 g was used for an indentation time of 10 s. Several measurements at different locations on the Zn coating surface were performed in order to determine an average hardness value. The procedure for hardness measurements involved electrodeposition of a thick Zn coating ($t_D = 100$ h) from the same electrolyte and in the same conditions applied in linear CV and PO described above. The Zn samples were embedded in an epoxy resin, subjected to a metallographic refining and rinsed with ultrapure water before measuring the hardness.

3. Results and discussion

3.1. *Zn electrodeposition on Si(n) and ITO by CV*

Current–potential curves were recorded in order to choose the optimal working conditions for Zn grown both on ITO and n-Si substrates. Figure 1(a) shows the voltammogram for a bare n-Si substrate at 30 °C in the background electrolyte (KAc, pH = 6.3).

Two processes are observed: for potentials more anodic than +0.4 V oxidation of the electrode surface takes place and for potentials more cathodic than −1.35 V the hydrogen evolution reaction starts. This value is 0.760 V more negative than the theoretic value (−0.590 V) due to the hydrogen overpotential on the Si(n). Figure 1(b)–(f) shows the voltammograms of Si(n) in $ZnAc_2$ solution (0.496 M, pH = 6.3) for different cathodic potential limits. For $E = 1.1$ V a current corresponding to the deposition of Zn is observed in the cathodic scan, while in the anodic scan there is a

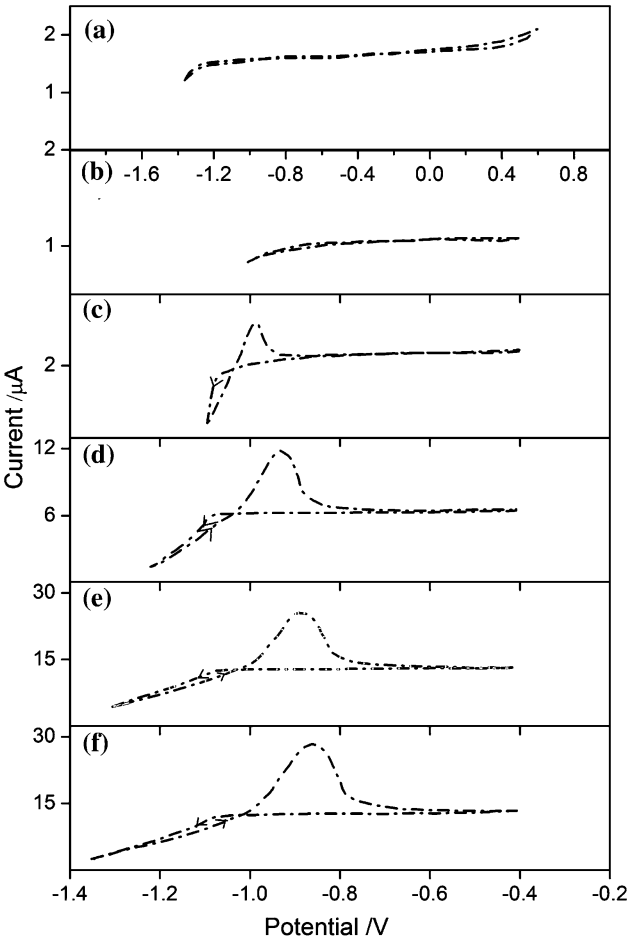

Fig. 1. CV for n-Si: (a) in a KAc dissolution (pH = 6.3); (b–f) in a 0.496 M $ZnAc_2$ dissolution ($v = 10$ mV s^{-1}).

Table 1. Several values for cathodic (E_F) and stripping (E_P) potentials

E_F/V	E_P/V
−1.10	−0.98
−1.15	−0.94
−1.20	−0.92
−1.25	−0.89
−1.30	−0.86
−1.35	−0.85
−1.80	−0.77

Electrodeposition under more negative E_F implies more anodic stripping potentials due to an increase in stability.

current peak due to the redissolution of the electrodeposited Zn according to the following reaction:

$$Zn^{+2} + 2e^- \leftrightarrow Zn^0$$

As the cathodic potential limit is more negative than −1.1 V the cathodic current is seen to be greater in the anodic scan than in the cathodic scan, due to the increase in the exposed area as electrodeposition proceeds. On the other hand, stripping takes place at more anodic potentials (Table 1), indicating an increase in stability as the Zn bulk deposit grows.

For $E_F = -1.35$ V the only process that takes place on the electrode is the reduction of Zn^{+2} ions from the ionic dissolution, and no hydrogen evolution is observed. The redox potential of the Zn/Zn^{2+} couple ($C_{Zn+2} = 0.496$ M, pH = 6.3) is −0.969 V vs. Ag/AgCl. If this value is compared with the redox potential value for the H^+/H_2 couple at the same pH ($E_{H+/H_2} = -0.590$ V) it is deduced that Zn cannot be deposited without the simultaneous evolution of hydrogen. However, the theoretic potential values do not consider the substrate upon which the reaction takes place, i.e. it has not been taken into account that it may be necessary to impose an overpotential in order for both reactions to take place on the Si(n) electrode. Experimentally it has been found that the activation overpotential (η activation) for hydrogen evolution on Si(n) is 0.760 V (Figure 1(a)), i.e. the hydrogen reaction does not take place before a potential of $E = -1.35$ V.

Furthermore, there is practically no nucleation overpotential for the deposition of Zn on Si, since deposition starts at potentials more negative than −1.05 V (Figure 1(b)), a value close to the theoretical redox potential value ($E_{Zn/Zn^{2+}} = -0.969$ V). Therefore, between −1.05 and −1.35 V it is possible to deposit Zn on Si(n) without the interference of hydrogen evolution. Consequently, the Zn samples on Si(n) grown by CV were obtained applying the potential range −1.05 to −1.35 V at a scan rate of 10 mV s^{-1}. Under these conditions the redissolution of the deposit is prevented. Growth proceeds under kinetic control. Voltammograms were recorded for ITO substrates in the same concentration and temperature conditions (not shown). In the absence of electroactive substances ($ZnAc_2$), the hydrogen evolution reaction starts at $E = -1.2$ V and Zn deposition begins at −1.0 V. The stripping current peak is observed at a potential of −0.550 V. However, in this case degradation of the electrode material occurs below $E = -1.055$ V. Zn electrodeposition was carried out between −0.850 and −1.055 V, at a scan rate of 10 mV s^{-1}. As in the former case the electrodeposition process does not involve redissolution.

Deposition was performed at 25 and 30 °C. A temperature increase of 5 °C hardly affects the voltammograms, and therefore the potentials applied to obtain deposits at $T = 30$ °C were the same as at $T = 25$ °C. However, this temperature increase increases the Zn^{2+} ion diffusion rate towards the electrode surface and also the surface diffusion, giving rise to more compact deposits.

3.2. *Zn electrodeposition on Si(n) and ITO by PO*

Figure 2 shows the voltammogram for Zn deposition on Si(n) when the cathodic potential limit is −1.8 V. When E_F is more negative than −1.35 V, the deposition of Zn would have to take place simultaneously with the evolution of hydrogen, as explained above. However, only the deposition process takes place, because once a Zn monolayer has been deposited on the Si(n) electrode the hydrogen reaction would take place on Zn and not on Si. The Zn–H binding energy is relatively weak (< 10 kJ mol^{-1}) and therefore its rupture is not the determining step of the hydrogen development rate on Zn but the charge transfer due to the proton:

$$Zn + H^+ + 1e^- - - \rightarrow ZnH_{ads}$$

$$ZnH_{ads} + H^+ + 1e^- \rightarrow Zn + H_2$$

Bearing in mind that the exchange current density in the i_0 equilibrium is of the order of 10^{-6} A m^{-2} [18] and the hydrogen overpotential on Zn is several hundreds of millivolts ($\eta \approx 0.7\,V, E_{H_2/Zn} \approx -1.8\,V$), it is possible to electrodeposit Zn on Si(n) without the interference of

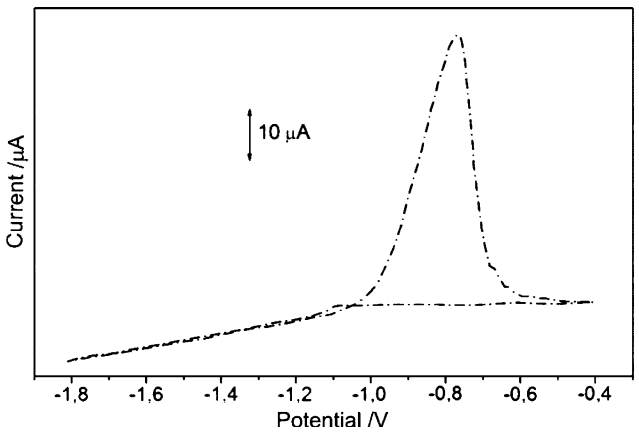

Fig. 2. CV for a n-Si substrate in 100 g l^{-1} $ZnAc_2$ aqueous solution at pH = 6.3 ($v = 10$ mV s^{-1}).

the hydrogen evolution reaction in a broad range of potentials.

Therefore, the electrodeposition of Zn on a Si(n) substrate by means of a square wave PO is achieved by applying a repetitive potential pulse between a deposition potential $E_{on} = -1.8$ V for $t_{on} = 1$ ms and $E_{off} = -1.05$ V for 10 ms (t_{off} = time interval between two pulses in which the system relaxes). The pause-to-pulse ratio is 10, a high value in order to reduce the value of $\omega(\eta$ diffusion control$/\eta$ activation) in order to obtain less scattered deposits [19]. The pulse frequency is 90.9 Hz. These values are within the optimum range to obtain compact deposits since the depletion in the diffusion layer at the end of the pulse is small, keeping the surface concentration practically constant throughout the pulse duration ($t = 1$ ms) and thus free from the influence of mass transport limitations. Besides, for a deposition potential of $E = -1.8$ V there is kinetic control, as can be seen in the voltammogram (Figure 2). For potentials more anodic than $E = -1.05$ V, stripping of the deposit takes place. At times it may be positive for the most unstable parts of the deposit formed during the cathodic pulse to redissolve during the relaxation time. However, in our case we have chosen a relaxation potential at which the deposit does not redissolve, allowing the structure to relax due to the diffusion of Zn adatoms towards superficial sites with a greater coordination index. The system has sufficient time (10 ms) to reach this thermodynamically more stable state. During the *on time* the formation of Zn nuclei takes place, and during the *off time* recrystallisation occurs, leading to the obtainment of larger grains. For samples on ITO substrates, $E_{deposition} = -1.05$ V and $E_{off} = -0.85$ V.

Zn electrodeposition was performed at two different temperatures: 25 and 30 °C. An increase in the temperature during the deposition process supposes an increase in the diffusion of the ions in solution as well as an increase in the diffusion of the adatoms to occupy more stable positions, giving rise to denser deposits.

3.3. *Morphology of Zn bulk deposits obtained by CV at T = 25 and 30 °C*

SEM images (Figure 3(a), (b)) show the initial steps of a Zn electrodeposit obtained by CV at 25 and 30 °C, respectively. The Zn initially grows to form large randomly oriented needle crystals, giving rise to a fine network of wires. The model of growth implies that Zn^{2+} ions (adions) are discharge to form adatoms once they have found a growth cluster exhibiting isotropic growth with larger and thin branches.

According to previous chronoamperometric experiments [20], the diffusion coefficient of Zn^{2+} ions and the nucleation density (N_0) increase with the rise in temperature. This means that the Zn ions are reduced to form adatoms more quickly at high temperature. Furthermore, the possibility that adatoms attached to the growing cluster can diffuse and reach stable sites with a greater number of coordination atoms also increases with the temperature. Therefore at 30 °C, due to the increase in the surface diffusion rate, the adatoms after being incorporated in the deposit structure move towards the voids, giving rise to smoother deposits (Figure 3(b)). In this case the Zn also shows isotropic growth with less cutting branches than in Figure 3(a).

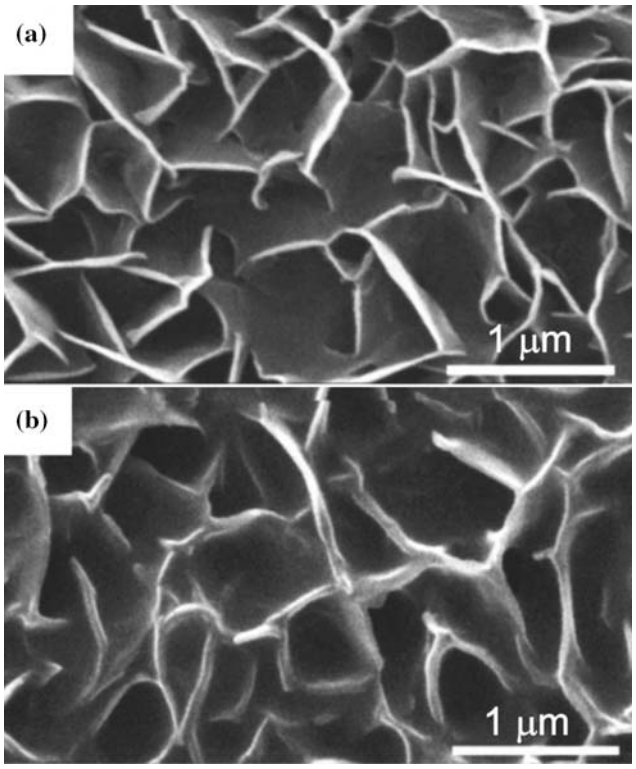

Fig. 3. Bulk deposits obtained by CV for 8 h on Si (n) substrate: (a) $T = 25$ °C; (b) $T = 30$ °C.

Figure 4(a) and (b) show SEM micrographs for thick Zn deposits obtained at 25 and 30 °C, respectively. The grain growth direction is parallel to the Si(n) substrate containing packets of hexagonal plates, each with a pronounced layered structure.

At 25 °C (Figure 4(a)) smaller hexagonal crystallites are seen to nucleate on the larger hexagonal platelets. A model illustrating this type of growth has been presented by Yan et al. [7], who propose a rapid growth direction of the crystallites parallel to the basal plane (002) and a slower growth direction for crystallites parallel to the prismatic plane (100). Hexagonal Zn platelets have been obtained in sulphate [7], acetate [20] and chloride [21] solutions.

The effect of a temperature increase to 30 °C (Figure 4(b)) is that, although the deposit structure shows the same morphology as at 25 °C, in this case the platelike crystals develop integrally to form regular hexagons. The irregular growth shown at 25 °C, according to Kossel's theory, is due to the fact that the surface diffusion rate of the Zn adatoms towards thermodynamically more stable sites is slow, and they are trapped by the adatoms formed subsequently, giving rise to steps and kinks [20].

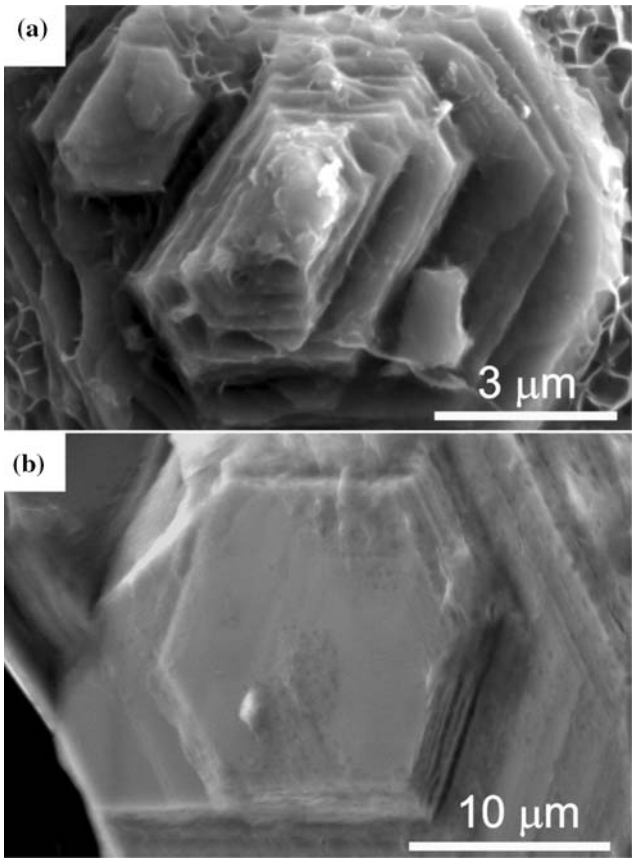

Fig. 4. Bulk deposits obtained by CV for 20 h on Si(n) substrate at (a) $T = 25$ °C and (b) $T = 30$ °C.

3.4. *Morphology of Zn bulk deposits obtained by PO at $T = 25$ and 30 °C*

SEM micrographs (Figure 5(a) and (b)) show the initial stages of growth for a Zn electrodeposit obtained in PO conditions at $T = 25$ and 30 °C, respectively.

The morphology of the deposit continues to consist of fibres but the height of these fibrous structures is much less than if the deposit is obtained in CV conditions (Figure 3). Remarkable differences can be seen between the samples obtained with the two methods (Figures 3 and 5). In the former (PO) the wires are discerned on a dense background while in the latter (CV) the wires are only the crests of enveloping layers.

If the SEM images at 25 and at 30 °C are compared (Figure 3 and 5), it is seen that the height of the deposits is greater in those obtained by CV than in those obtained by PO, at both temperatures. The reason for this is that with CV the fibres grow progressively as the number of cycles increases, whereas in PO conditions there is a relaxation time between successive pulses which allows the relaxing of the structure.

An increase in the temperature to 30 °C (Figure 5(b)) gives rise to a denser deposit with wider, more rounded and smoother fibres than at $T = 25$ °C (Figure 5(a)), again due to an increase in the nucleation density (N_0), in the Zn ion diffusion coefficient, and in the superficial Zn adatom diffusion rate.

Figure 6 shows SEM micrographs for thick Zn deposits obtained by PO. It can be seen that the grains contain packets of hexagonal plates whose growth direction is practically perpendicular to the n-Si substrate. Figure 6(b) shows the effect of a 5 °C temperature increase on the thick Zn deposits. The deposit at 30 °C appears smoother and with more rounded profiles than at 25 °C.

3.5. *X-ray diffraction*

The microstructure of the Zn samples grown on n-Si substrates was studied by diffractometric analysis. Figure 7(a) shows the diffractogram of a Zn sample obtained by CV at 25 °C on Si (n). No peaks related to the substrate can be appreciated since the spectrum was collected at grazing incidence angle. The highest reflection intensities of low angle planes corresponded to the (002), (100) and (101) preferential orientations.

It is noteworthy that the diffraction peaks are attributed to the known hexagonal prism (wurtzite) structure phase of Zn. The intensity ratio of (100) with respect to (101) peaks is variable, in the range 0.2–0.3, in contrast to standard bulk Zn, for which the ideal intensity ratio between (100) and (101) peaks is 0.4 for a random specimen.

If Zn is deposited in PO conditions the diffractograms show that the intensity of the pyramidal planes is the highest and simultaneously that of the basal plane (002) and prismatic planes (100) are the lowest (Figure 7(b)). In fact, the measured intensity ratio between (100) and (101) preferential orientations has very low values (0.1).

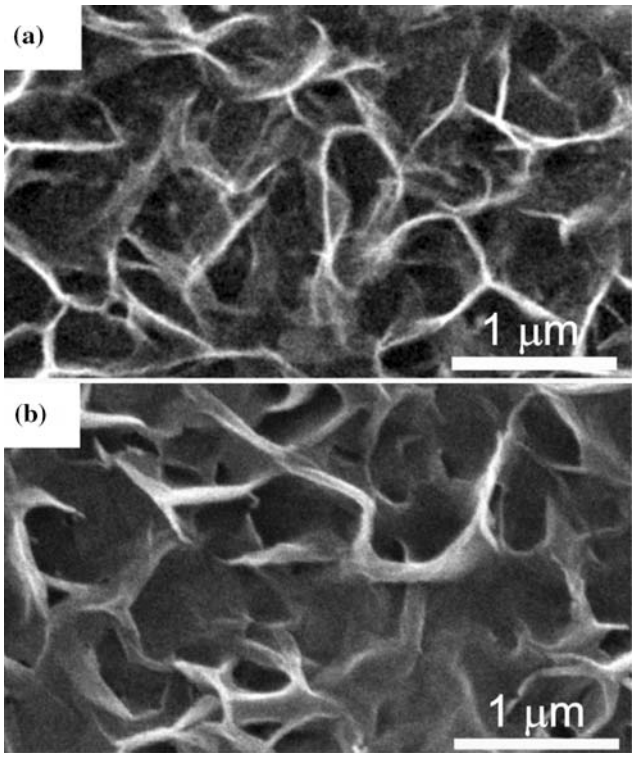

Fig. 5. Bulk deposits obtained by PO for 8 h on Si(n) substrate at (a) 25 °C and (b) 30 °C.

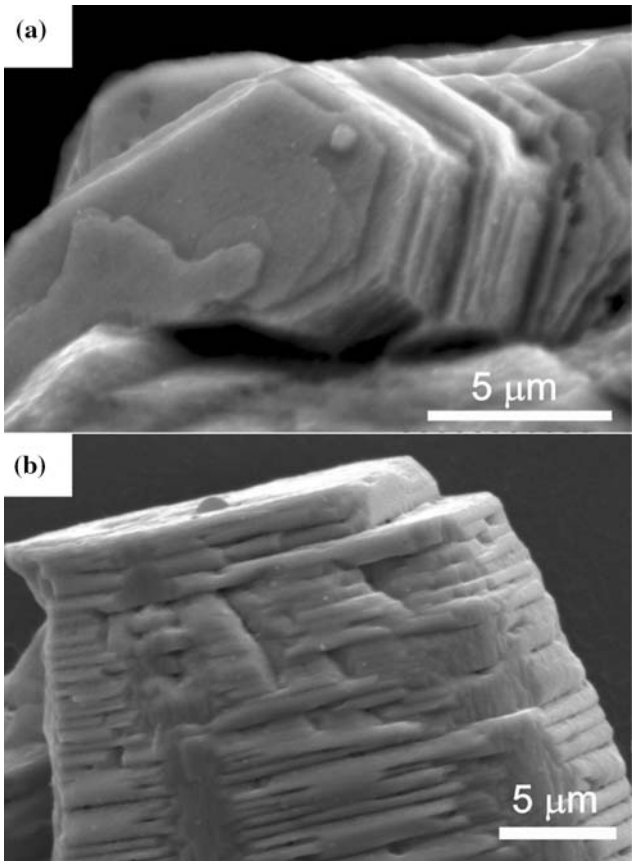

Fig. 6. Bulk deposits obtained by PO on Si(n) substrate for 20 h: (a) $T = 25$°C. (b) $T = 30$ °C.

With long deposition times (100 h), i.e. for greater thicknesses, there is an increase in the diffraction peak corresponding to the basal plane (002) and the intensity of the (100) is depressed compared to the values predicted for bulk Zn (Figure 7(c)). Therefore, if the diffraction originated from the growth plane decreases, compared with a randomly oriented powder, this may be interpreted as the Zn growing preferentially along the (100) axis [22] or equivalently, parallel to the (002) plane, which is consistent to the observed strongest (002) peak.

The average Zn crystallite size for Zn electrodeposited under PO or CV conditions, at a temperature of 25 or 30 °C, was calculated by considering the line broadening of the diffraction peaks. The apparent grain size was obtained by applying Scherrer's equation:

$$D_{hkl} = \frac{K\lambda}{\beta \cos\theta} \cdot \frac{360}{2\pi}$$

where D_{hkl} is the average dimension of the crystals in the normal direction of the planes that diffract the radiation. K is 0.9 when it is assumed that the particles are spherical. λ corresponds to the copper Kα radiation wavelength. In order to make this calculation, use has been made of the weighted mean between $\lambda\alpha_1 = 1.54056$ Å and $\lambda\alpha_2 = 1.54439$ Å. β is the FWHM of the diffraction peak corrected for the instrumental broadening and 2θ is the diffraction angle. The grain size, D_{hkl}, was calculated for each one of the orientations reflected in the diffractogram, giving an average value of 733 Å for electrodeposits obtained under CV conditions at 25 °C.

Table 2. Grain size (Å) values for electrodeposits obtained by CV and PO at different temperatures

T/°C	PO	CV
25	682	733
30	859	960

If the Zn is electrodeposited at a temperature of 30 °C the average size of the crystallite, calculated from the X-ray diffraction peaks, is 960 Å.

Table 2 shows a summary of calculated grain size values for the two electrochemical methods used at two different temperatures. It may be concluded that the grain size increases as the temperature rises as a consequence of an increase in the superficial diffusion rate of the Zn adions or adatoms.

The results also show, in accordance with the theory [18], that electrodeposition in pulse conditions yields smoother uniform surfaces with finer grains as a result of higher instantaneous current densities. In contrast, if the Zn deposit is obtained by CV the grain size is greater since the nuclei generated under these conditions grow as the number of scans increases.

3.6. *Hardness evaluation*

The hardness of the Zn deposits obtained by PO is greater than that of the Zn deposits obtained by CV, irrespective of the temperature (Table 3). As has already been noted, the crystallite size obtained by the PO method is smaller than that obtained by CV, irrespective of the temperature. Therefore, an increase in the hardness of these samples may be attributed to the reduction in the grain size of the nanocrystalline (nc) Zn.

On the other hand, an increase in temperature leads to an increase in the grain size, irrespective of the method applied to obtain the Zn deposit (Table 2), and therefore a decrease in the hardness of the electrodeposit.

The values obtained for the hardness of nc Zn deposits are slightly lower than those obtained for nc Zn produced by different techniques and are similar to polycrystalline Zn. The reason is that in our case, the nc Zn electrodeposit has a larger nanograin size (682–960 Å) than the nc Zn produced by vapour deposition (50–500 Å), mechanical attrition (200–300 Å) and laser ablation (50–300 Å), whose hardness is greater [6].

Table 3. Hardness value (Vickers) for electrodeposits obtained by CV and PO at different temperatures

T/°C	PO	CV
25	39.0	36.6
30	35.4	32.0

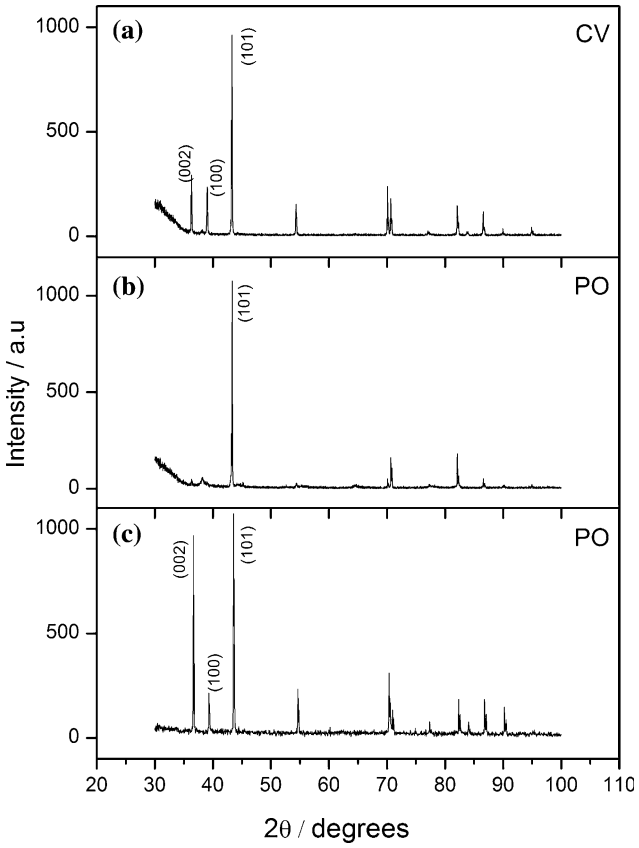

Fig. 7. XRD of Zn samples obtained at (a) 30 °C by CV, (b) 25 °C by PO and (c) 25 °C by PO for 100 h.

If these results are compared with the morphology and structure of the deposits, it is seen that the hardest coatings are the most uniform.

4. Conclusions

Zn deposited by means of CV and PO on ITO and Si(n) substrates from an acetate-based electrolyte is formed, in the initial stages, by large randomly oriented needle crystals whose shape and density depends on the temperature and the processing method used.

The thick deposits are formed by grains that contain hexagonal plates, each with a laminar structure. For electrodeposits grown on n-Si substrates by CV there is a rapid growth direction of the crystals parallel to the basal plane (002), and a slower growth direction parallel to the prismatic plane (100). For deposits obtained by PO the maximum diffraction intensity corresponds to the pyramidal plane (101). However, for long deposition times the growth direction is (100), which corresponds to the basal plane (002).

On the other hand, the PO method yields smaller grains and higher hardness values than CV, irrespective of the temperature.

References

1. T. Watanabe, *Nano-Plating: Microstructure Control Theory of Plated Film and Data Base of Plated Film Wicrostructure*. Chapter 7 (Elsevier, 2004), pp. 358–369.
2. R. Sato, *J. Electrochem. Soc.* **106** (1959) 206.
3. T. Hilber, P. Letonja, R. Marr, P. Pölt and M. Siebenhofer, *Part. Syst. Charact.* **19** (2002) 342.
4. J. Yu, Y. Chen, H. Yang and Q. Huang, *J. Electrochem. Soc.* **146** (1999) 1789.
5. J. Lee and Y. Tak, *Electrochem. Solid State Lett.* **4** (2001) C63.
6. Kh. Saber, C.C. Kock and P.S. Fedkiw, *Mater. Sci. and Eng.* **A341** (2003) 174.
7. H. Yan, J. Downer, P.J. Boden and S.J. Harris, *J. Electrochem. Soc.* **143** (1996) 1577.
8. A.C. Magalhaes, R.C.B. Da Silva, N.M. Cassiano and M.D. Capelato, *Bull. Electrochem.* **18** (2002) 193.
9. S. Arouete, K.F. Blurton and H.G. Oswin, *J. Electrochem. Soc.* **116** (1969) 166.
10. D. Grier, E. Ben-Jacob, Clarke Roy and L.M. Sander, *Phys. Rev. Lett.* **56** (1986) 1264.
11. K. Nomura, N. Shibata and M. Maeda, *J. Electrochem. Soc.* **149** (2002) 76.
12. C.A. Loto and I. Olefjord, *Cor. Prev. Contr.* (1990) 158.
13. B.C. Tripathy, S.C. Das, G.T. Hefter and P. Singh, *J. Appl. Electrochem.* **28** (1998) 915.
14. D.J. MacKinnon and J.M. Brannen, *J. Appl. Electrochem.* **12** (1982) 21.
15. Y.B. Yim, W.S. Hwang and S.K. Hwang, *J. Electrochem. Soc.* **142** (1995) 2604.
16. K. Raeissi, A. Saatchi and M.A. Golozar, *J. Appl. Electrochem.* **33** (2003) 635.
17. B.H. Juarez, C. Lopez and C. Alonso, *J. Phy. Chem. B* **108** (2004) 16708.
18. A.J. Appleby, M. Chemla, H. Kita and G. Bronoel, *in* A.J. Bard (ed). 'Encyclopedia of the Electrochemistry of the Elements', Vol. IXA (Marcel Dekker, 1982), 383 pp.
19. K.I. Popov and M.D. Masimovic, *in* B.E.Conway, J. O'M. Bockris and R. E White (Eds.), 'Electrochemistry', Vol. XIX (Plenum Press, New York 1989), 193 pp.
20. J. Yu, L. Wang, L. Su, X. Ai and H. Yang, *J. Electrochem. Soc.* **150** (2003) C19.
21. E. Gómez and E. Vallés, *Bull. Electrochem.* **10** (1994) 477.
22. C. Tang, Y. Bando, Z.W. Liu and D. Golberg, *Chem. Phys. Lett.* **376** (2003) 676.